# Murine macrophage choline metabolism underpins IL-4 polarization and RELMα up-regulation

Peyman Ghorbani[1,2*], Sang Yong Kim[3*], Tyler K.T. Smith[1,2], Lucía Minarrieta[1,2], Marisa K. Kilgour[1,2], Maja Ilijevska[1,2], Irina Alecu[1,2,4], Shayne A. Snider[1], Kaitlyn D. Margison[1], Julia R.C. Nunes[1,2], Daniel Woo[3], Ciara Pember[1,2], Conor O'Dwyer[1,2], Julie St-Pierre[1,2,4], Steffany A.L. Bennett[1,2,4-6], Meera G. Nair[3#], Morgan D. Fullerton[1,2,5#]

[1] Department of Biochemistry, Microbiology and Immunology, Faculty of Medicine, University of Ottawa, Ottawa, ON, Canada

[2] Centre for Infection, Immunity and Inflammation, University of Ottawa, Ottawa, ON, Canada

[3] Division of Biomedical Sciences, School of Medicine, University of California Riverside, Riverside, CA, USA

[4] Ottawa Institute of Systems Biology, University of Ottawa, Ottawa, ON, Canada

[5] Centre for Catalysis Research and Innovation, University of Ottawa, Ottawa, ON, Canada

[6] University of Ottawa Brain and Mind Institute, University of Ottawa, Ottawa, ON, Canada

* denotes equal contribution, # denotes equal corresponding authorship

Running Title: Choline sustains macrophage IL-4 responses

## Abstract

Choline is an essential nutrient and in macrophages, mainly supports phosphatidylcholine (PC) synthesis. Cellular uptake and incorporation of choline into PC is critical for LPS-induced macrophage inflammation. Here, we examined choline metabolism in the context of IL-4 polarization of mouse macrophages *in vitro* and *in vivo*. Like LPS, IL-4 increased the levels of choline transporter-like protein 1, the rate of choline uptake, and incorporation into PC. Targeted lipidomics analysis revealed higher PC content in IL-4-polarized macrophages, with enrichment in low-saturated species. Pharmacological inhibition of choline metabolism significantly suppressed the transcription of certain hallmark IL-4 genes (*Retnla*) but not others (*Chil3*, *Mrc1*, *Arg1*). Blocking choline metabolism diminished the expression and secretion of RELMα protein (encoded by *Retnla*), while also limiting PD-L2 up-regulation and increasing PD-L1 expression. *In vivo* administration of RSM-932a, a choline kinase inhibitor, caused a dramatic shift in the peritoneal immune cell profile and up-regulated macrophage CD86 and PD-L1, while down-regulating CD206 and PD-L2. Strikingly, blocking choline metabolism lowered RELMα expression in multiple cell-types and tissues in naïve mice as well as mice infected with the helminth pathogens *Heligmosomoides polygyrus* and *Nippostrongylus brasiliensis*. There were no changes in pathogen burden or clearance in the two separate helminth models. In contrast, in dextran sulfate sodium-induced colitis, loss of colon length as a marker of inflammation was mitigated by choline metabolism inhibition. These data demonstrate a critical link between choline and macrophage effector functions and suggest that targeting choline metabolism could be leveraged to fine-tune immunopathology.


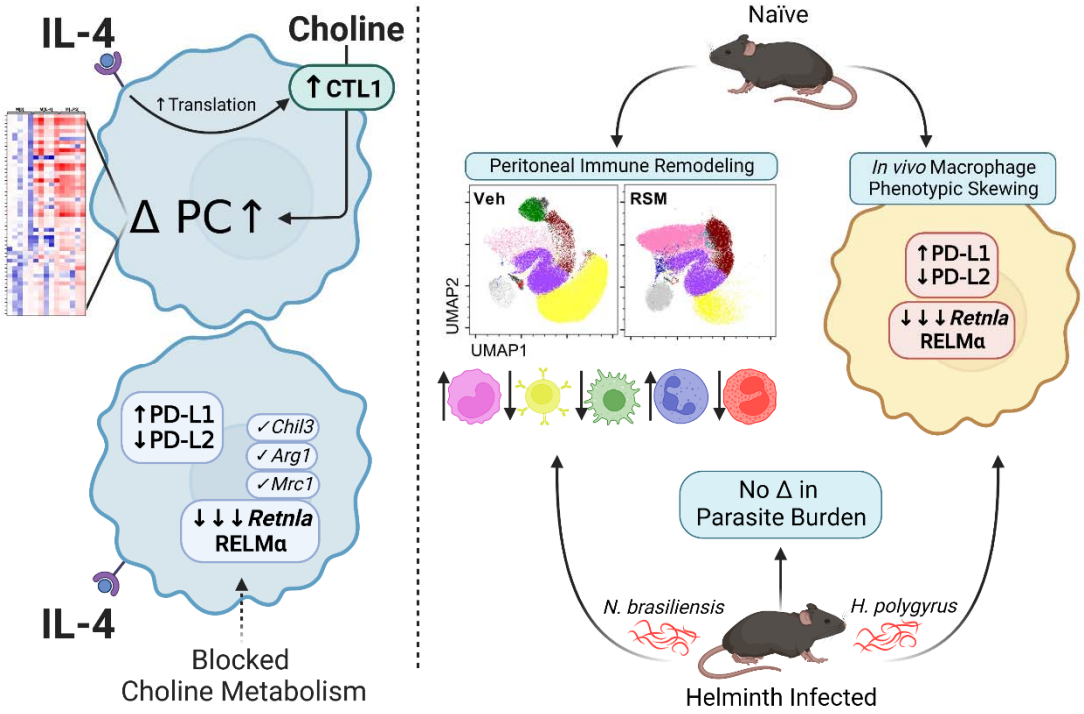

## Introduction

Macrophages represent a heterogeneous and plastic subset of innate immune cells that perform critical homeostatic, surveillance and effector tasks in almost all tissues.[1] They can dynamically respond to diverse endogenous and exogenous cues, including nutrient and energy availability. Metabolic programming can directly drive macrophage function but can also be rewired in response to various stimuli.[2] While we continue to expand our understanding of how energy-generating pathways and their intermediates underpin immunometabolic function, the importance of nutrients in macrophage biology remains underexplored.

Choline is a quaternary amine and essential nutrient that can form the main eukaryotic phospholipid class, glycerophosphocholines (most abundant of which is phosphatidylcholine (PC)), or form acetylcholine in cholinergic tissues.[3] Additionally, methyl groups from choline contribute to one-carbon metabolism after its mitochondrial oxidation. Given its positive charge, choline requires facilitated transport across cellular membranes, representing the first but least studied step in its metabolism. In immune cells, choline transporter-like protein 1 (*Slc44a1*/CTL1) is responsible for the majority of choline uptake.[4,5] Upon uptake, choline is thought to be rapidly phosphorylated by choline kinase (Chkα/Chkβ) and is then committed to the PC biosynthetic (CDP-choline/Kennedy) pathway.[3,6]

Phospholipid biosynthesis is indispensable for membrane biogenesis, which plays an important role in cellular differentiation and phagocytosis.[7] The first insight into the potential role of choline in macrophage function came over twenty years ago with the observation that deletion of myeloid *Pcyt1a*, encoding the rate-limiting enzyme in PC synthesis, diminished adaptive responses to endogenous stimuli (free cholesterol)[8] and impaired the secretion of pro-inflammatory cytokines from macrophages.[9] Recent lipidomic analyses of cultured macrophages demonstrated sweeping alterations to phospholipid composition and content in response to various inflammatory stimuli.[4,10-12] To begin to address the specific roles of choline as a regulator of macrophage functions, we and others have shown that polarization with the bacterial endotoxin lipopolysaccharide (LPS; termed M[LPS]) in primary mouse macrophages leads to increased choline uptake and PC synthesis in an *Slc44a1*-dependent manner.[4] While inhibiting choline uptake and metabolism led to more pronounced inflammatory responses in M[LPS], whether choline metabolism is regulated and how it may alter macrophage phenotype in response to Th2 cytokine exposure remains unknown.

Interleukin-4 (IL-4), along with IL-13, is a signature cytokine of type 2 inflammatory responses.[13] In addition to being widely used to polarize macrophages *in vitro* (termed M[IL-4]), secretion of these cytokines *in vivo* is a critical response triggered by invading macroparasites or allergens.[14] Since it is now appreciated that macrophage inflammatory and metabolic programs exhibit a dichotomy in response to prototypical pro- and anti-inflammatory stimuli, we sought to characterize the interplay between choline metabolism and IL-4-mediated polarization of macrophages. Interestingly, we found that identical to LPS, choline uptake and incorporation into PC was augmented in M[IL-4]. Moreover, when choline uptake and metabolism was inhibited, we observed select but striking differences in IL-4-specific responses, underpinned by a dramatic reduction in RELMα both *in vitro* and in mouse parasitic helminth infection.

## Materials and Methods

*Animals*

Mice (C57BL/6J) were originally purchased from Jackson Laboratories (Stock no. 00064) and bred in a pathogen-free facility in the University of Ottawa animal facility or acclimated for 7 days prior to *H. polygyrus* infection at the University of California Riverside. Mice were maintained on a 12-hour light dark cycle (lights on at 7:00 am) and housed at 23°C with bedding enrichment. Male and female mice ages 8-16 weeks were used for the generation of primary macrophages as described below. All animal procedures were approved by the University of Ottawa Animal Care Committee and the University of California Riverside Institutional Animal Care and Use Committee (protocol A-20210017).

*Isolation, culturing and polarization of bone marrow-derived macrophages*

Bone marrow-derived macrophages (BMDM) were isolated and cultured as previously described.[15,16] Briefly, bone marrow cells were obtained from the femur and tibia by centrifugation.[4] Cells were differentiated into macrophages using 15-20% L929-conditioned media in complete DMEM (Wisent) containing 10% FBS (Wisent), 1% penicillin/streptomycin. Cells were plated into 15 cm dishes and allowed to differentiate for 6-8 days. Cells were lifted by gentle scraping, counted, and seeded into culture plates for experiments at $1x10^6$/mL. Cells were treated for 24 h with DMSO as vehicle or inhibitors: hemicholinium-3 (Sigma-Aldrich), RSM-932a (Cayman Chemicals). Macrophages were polarized with 20 ng/mL recombinant IL-4 (Peprotech or Roche) or 100 ng/mL LPS (*E. coli*:B4, Sigma-Aldrich). Choline-free DMEM was formulated by preparing nutrient-deficient DMEM (US Biologicals, D9809) according to manufacturer's instructions and supplementing with sodium pyruvate (Gibco), *myo*-inositol, L-methionine, and calcium D-pantothenate (Sigma-Aldrich).

*Choline uptake, incorporation, uptake inhibition and degradation*

The rate of choline uptake, incorporation into PC, uptake inhibition and degradation were determined in M[0] and M[IL-4] using $^3$H-choline chloride (Perkin Elmer) as previously described.[4]

*High-performance liquid chromatography electrospray ionization tandem mass spectrometry (LC-ESI-MS/MS) Lipidomics*

Cells were counted, pelleted, and frozen at -80°C in 15 mL Falcon tubes for 24 h. Pellets were resuspended in 1 mL sodium acetate using a syringe pipette and transferred to Kimble tubes. Tubes were washed two times in sodium acetate to recover all material. All pipette tips were autoclaved glass. MS grade lipid standards, LPC(13:0/0:0) [90.7 ng Avanti Polar Lipids], PC(12:0/13:0) [100 ng, Avanti Polar Lipids], and SM(d18:1/18:1-D9) [75 ng Avanti Polar Lipids] were added to the homogenate at time of extraction. Lipids were extracted using a modified Bligh and Dyer[17] protocol at a final ratio of acidified methanol/chloroform/sodium

acetate of 2:1.9:1.6 as described.[18,19] The organic phase was retained and the aqueous phase successively back-extracted using chloroform three times. The four organic extracts were combined and evaporated at room temperature under a constant stream of nitrogen gas. Final extracts were solubilized in 300 µL of anhydrous ethanol (Commercial Alcohols) and stored under nitrogen gas at -80°C in amber vials (BioLynx).

Lipid quantification was performed on an Agilent 1290 Infinity II liquid chromatography system coupled to a QTRAP 5500 triple quadrupole-linear ion trap mass spectrometer using a Turbo V ion source (AB SCIEX) in positive ion mode. Reverse phase chromatography used a binary solvent gradient of solvent A (water with 0.1% formic acid (Fluka) and 10 mM ammonium acetate (OmniPur)) and solvent B (acetonitrile (J.T. Baker) and isopropanol (Fisher) at a ratio of 5:2 v/v with 10 mM ammonium acetate and 0.1% formic acid). The LC gradient used for glycerophosphocholine analysis started at 30% Solvent B, reached 100% Solvent B at 8 minutes, and remained at 100% B for 45 min. At 45 min, composition was returned to 30% Solvent B and the column was regenerated for 15 min. Samples were prepared for HPLC injection by mixing 5 µl of lipid extract with 2.5 µL of an internal standard mixture consisting of LPC(O-16:0-D4/0:0) [2.5 ng, Cayman], LPC(O-18:0-D4/0:0) [2.5 ng, Cayman], PC(O-16:0-D4/2:0) [1.25 ng, Cayman] and PC(O-18:0-D4/2:0) [1.25 ng Cayman] in EtOH, and 16 µL of Solvent A. Three µL autosampler injections at 4°C were pumped over a nanobore 100 mm x 250 µm (i.d.) capillary column packed in-house with ReproSil-Pur 200 C18 (particle size of 3 µm and pore size of 200 Å, Dr. A. Maisch, Ammerbruch). Transition lists were established using precursor ion scan interrogating a diagnostic fragment ion at m/z 184.1, corresponding to the phosphorylcholine headgroup of the protonated molecular ion ($[M+H]^+$). Once all detectable species were established in precursor ion discovery mode, targeted lipid quantification was performed using selected reaction monitoring (SRM), monitoring transitions from $[M+H]^+$ to m/z 184.1. ESI-MS/MS acquisition and instrument control were performed using Analyst software (version 1.6.3, SCIEX). The ion source operated at 5500 V and 0°C. Nebulizer/heated gas (GS1/GS2), curtain gas, and collision gas (all nitrogen) were set to 20/0 psi, 20 psi, and medium, respectively, for GPC analysis. Compound parameters (declustering potential, entrance potential, collision energy, and collision cell exit potential) were individually optimized for each transition. MultiQuant software (version 3.0.2 AB SCIEX) was used for peak picking and processing quantitative SRM data. Bayesian Annotations for Targeted Lipidomics (BATL v2.7, https://www.complimet.ca/shiny/batl/) was used to assign peaks.[19] Peak areas were normalized to both cell number and either LPC(13:0/0:0) or SM(d18:1/18:1-D9) for PCs and SMs respectively to account for extraction efficiency and instrument response. Data are expressed as pmol equivalents per $10^6$ cells.

The identities of all lipid species in our samples were structurally determined in a single LC-ESI-MS/MS analysis of quality control samples composed of an equi-volume pool of all samples analyzed. SRM was used as a survey scan to trigger information dependent acquisition of EPI spectra in the linear ion trap. After acquisition, the EPI spectra were examined for structural determination.

*Wound healing*

3T3-L1 fibroblasts were passaged in complete DMEM, plated in ImageLock plates (Essen Bioscience) and grown to confluency. Macrophages were pre-treated with vehicle or HC3 for 24 h, washed with PBS, and supernatants were collected after a further 24h in complete DMEM ± 20 ng/mL IL-4. A scratch wound was made in each well of 3T3-L1 fibroblasts, wells were gently washed with warm PBS, and supernatants were added to 4 or 5 replicate scratch wound wells. Wound healing was monitored hourly for >24 h on an IncuCyte ZOOM system (Essen Bioscience).

*Flow cytometry*

Macrophages were plated in 6-well plates and treated with DMSO or HC3 (250 µM) for 48 h. After washing with PBS, cells were gently scraped or lifted with 10 mM EDTA in PBS. and blocked and stained with anti-CD16/32 (93, BioLegend) and Zombie Aqua dye (BioLegend) in PBS for 30 minutes on ice. Surface staining in PBA-E (1% BSA, 2 mM EDTA, 0.05% $NaN_3$ in PBS) was done for 20 minutes on ice. Cells were then fixed with 2% paraformaldehyde in PBS or Fix/Perm buffer (ThermoFisher) for 15 minutes. Intracellular staining was performed by permeabilization for 5 minutes on ice with 0.5% saponin in PBA-E (PBA-S) or permeabilization buffer (ThermoFisher) and subsequent staining with antibodies diluted in PBA-S. For intracellular phosphoprotein staining, cells were fixed directly after harvesting with -20°C phospho-flow fix buffer (4% paraformaldehyde/90% methanol in PBS). Surface antibodies were purchased from BioLegend or ThermoFisher: F4/80-PE (BM8), F4/80-AF488 (BM8), PD-L1-BV421 (10F.9G2), PD-L2-PE (TY25), RELMα-PerCP-eF710 (DS8RELM), Egr2-APC (erongr2), CD38-eF450 (90), pSTAT6(Tyr641)-APC (CHI2S4N), CD11b-APC-eF780 (M1/70), Ly-6C-PE-Cy7 (HK1.4), Ly-6G-AF647 (1A8), CD19-Pacific Blue (6D5), SiglecF-SB600 (1RMN44N), CD86-FITC (GL1). Unconjugated polyclonal rabbit anti-RELMα (Peprotech) was detected with goat anti-rabbit AF647 plus (ThermoFisher). Cells were washed and resuspended in PBA-E and acquired using LSR Fortessa or FACSCelesta flow cytometers (BD) and analyzed using FlowJo v10.7.2 (BD).

For *in vivo* helminth experiments, peritoneal exudate cells (PECs) were recovered in a total of 5 mL of ice-cold PBS. Cells were blocked with 0.6 µg Rat IgG and 0.6 µg anti-CD16/32 (93) for 5 minutes and stained for 30 minutes with antibodies to Ly6G (1A8), CD3e (145-2C11), PD-L1 (MIH6), CD86 (GL-1), CD4 (RM4-5), MERTK (2B10C42), CD301b (LOM-14), PD-L2 (TY25), CD5 (53-7.3), Ly6C (HK1.4), MHCII (M5/114.15.2) (BioLegend, San Diego, CA); CD8 (3B5), CD11b (M1/70) (Invitrogen); SiglecF (E50-2440) (BD Bioscience); CD206 (MR5D3) (BioRad). Cells were then washed and analyzed on a Novocyte (ACEA Biosciences) followed by data analysis using FlowJo v10.8.1 (BD). Frequencies or geometric mean fluorescence intensity (gMFI) was calculated.

*Transcript and protein expression*

Total RNA was isolated from BMDM using the TriPure reagent protocol (Roche Life Sciences). Isolated RNA was re-suspended in RNase/DNase-free water (Wisent). QuantiNova™ reverse

transcription kit (Qiagen) or ABM All-in-one RT kit (ABM) was used to synthesize cDNA according to manufacturer's instructions. To determine transcript expression, the QuantiNova™ Probe PCR kit (Qiagen) was used in combination with TaqMan primer-probe sets or BrightGreen Express MasterMix (ABM) with custom-designed primers. Comparative qPCR reactions were run on the Roto-Gene Q (Qiagen) or Stratagene MX3005p (Agilent). Relative transcript expression was determined using the delta-delta *Ct* method and normalized to *Actb* [20]. Following treatments, macrophage protein expression and phosphorylation status were assessed by immunoblotting as previously described.[4]

*Dextran sodium sulfate (DSS)-induced colitis*

Mice were provided 2-2.5% dextran sodium sulfate (MW 40-50 kDa, MP Biomedical) in drinking water *ad libitum* and treated intraperitoneally with vehicle (40% DMSO in PBS) or RSM-932a (3 mg/kg) every other day for 6 days and sacrificed at day 7. Colons were dissected out and measured with uniform tension by hanging the caecum from a clamp and applying a weight to the distal end. Liver, white adipose tissue, and 0.5-cm pieces of colon were snap-frozen in liquid $N_2$ or fixed in 10% neutral-buffered formalin (Sigma-Aldrich). Feces was collected daily and hemoccult was assessed by luminescence with ECL substrate (BioRad).

*RELMα ELISA*

Recombinant RELMα, polyclonal rabbit anti-RELMα capture, and polyclonal biotinylated rabbit anti-RELMα detection antibodies (all Peprotech) were used according to a previously described protocol.[21]

Heligmosomoides polygyrus *(*Hp*) and* Nippostrongylus brasiliensis *(*Nb*) infection models*

*Hp* and *Nb* life cycle was maintained in mice and rats, respectively, as previously described.[22,23] Mice were orally gavaged with 200 *Hp* L3 stage larvae or with PBS (naive group). Mice were infected subcutaneously with 500 *Nb* L3 stage larvae or injected with PBS (naïve group). Egg burden was measured at indicated day post-infection by counting eggs in feces with McMaster slide. To enumerate L5 stage *Hp*, the small intestines of infected mice were cut longitudinally, and larvae were isolated by fine forceps. *Nb* larvae were isolated after incubating the intestine in PBS for ≥ 2 hours at 37°C. Isolated larvae were counted on the petri dish with grids under the dissection microscope.

*RSM-932A*

RSM-932A (Cayman Chemical, Ann Arbor, MI) was reconstituted to 30 mg/mL in DMSO. For *in vivo* injection, RSM-932A was further diluted with DMSO and PBS to 1.5 mg/mL. Mice were injected intraperitoneally with 3 mg/kg of RSM-932A or 40% DMSO in PBS (vehicle group).

*Immunofluorescence staining*

Intestinal tissue was stored overnight in 4% PFA at 4°C. After 24 hours, tissue was removed from 4% PFA and incubated for 24 hours in 30% sucrose. Intestines were blocked in OCT and sectioned at 10 µm. Tissue sections were incubated with polyclonal rabbit anti-CD86 (ThermoFisher), APC-conjugated anti-RELMα (DS8RELM; Invitrogen), and biotinylated anti-CD206 (C068C2; BioLegend) antibodies overnight at 4°C. Tissue sections were then incubated with Cy3-conjugated goat anti-rabbit antibodies (Abcam) and Cy2-conjugated streptavidin (Jackson ImmunoResearch) for 2 hours at 4°C and mounted with VECTASHIELD HardSet Antifade Mounting Medium (Vector Laboratories) followed by imaging with BZ-X800 microscope (Keyence). Positive cells were counted by QuPath 0.3.2 (University of Edinburgh).[24]

*Statistical analysis*

Statistical analysis was performed in GraphPad Prism 9 (Dotmatics). Individual tests and sample sizes are described in figure legends.

## Results

*IL-4 upregulates choline metabolism in macrophages*

Macrophages only express two choline transporters, CTL1 and CTL2, and when polarized with LPS (M[LPS]) upregulate *Slc44a1* transcript and CTL1 protein expression.[4,5] Bone marrow-derived macrophages (BMDM) polarized with IL-4 (M[IL-4]) did not show increased *Slc44a1* or *Slc44a2* mRNA (Figure 1A); however, total (Figure 1B) and surface (Figure 1C) CTL1 protein expression was significantly augmented, suggesting post-transcriptional mechanisms. There were no changes in CTL2 protein levels. Polarization with IL-4 increased the rate of choline uptake (Figure 1D) and incorporation into PC (Figure 1E), without changing choline transport affinity or sensitivity to inhibition (supplemental Figure 1A-B). Moreover, while select phospholipases are upregulated in M[IL-4][25] we observed no difference in the rate of PC degradation (supplemental Figure 1C), suggesting an overall increase in cellular PC content in IL-4-polarized macrophages, which completely mirrored the effects of LPS polarization.[4]

*IL-4 increases PC content and alters choline containing phospholipid composition*

We performed targeted LC-MS/MS analysis of choline-containing phospholipids in naïve (M[0]), M[IL-4] and M[LPS]. Surprisingly, the typically divergent polarization states led to a symmetrical increase in PC levels, with no differences found in the level of sphingomyelin (Figure 2 and Figure S2A-B). With respect to lipid fatty acid composition of elevated PCs, we observed a significant increase predominantly in unsaturated and monounsaturated phospholipids (Figure 2B). Interestingly, there were also changes within the choline-containing lipidome in response to either IL-4 or LPS. The levels of platelet activating factors (PAF), their immediate precursor the lyso-PAFs (LPC(O)), as well as the lysophosphatidylcholines (LPCs) did not change in response to IL-4 but were significantly upregulated in M[LPS] (supplemental Figure 2C,D,H). The plasmalogen forms of PC, which have been demonstrated to be important for

downstream lipid signaling, showed divergent changes. Levels of plasmenyl PCs (PC(P)), structurally known as 1-alkenyl,2-acylglycerophosphocholines, as well as their immediate precursors (LPC(P)) were reduced in response to both stimuli while levels of plasmanyl PCs (PC(O)), known as 1-alkyl,2-acylglycerophosphocholines remained unchanged (supplemental Figure 2E-G).

*Inhibiting choline metabolism selectively impairs IL-4 polarization*

Since M[IL-4] are characterized by the expression of genes involved in dampening inflammation and promoting tissue repair, we sought to understand how limiting choline availability and metabolism may affect these well-known responses. We used an inhibitor of extracellular choline uptake (hemicholinium-3; HC3)[26] and an inhibitor of choline incorporation into PC, the choline kinase inhibitor RSM-932a (RSM). Pre-treatment of BMDM with HC3 for 24 h markedly impaired the induction of *Retnla* (Figure 3A), whereas other M[IL-4] hallmark genes like *Arg1*, *Mrc1* and *Chil3* (Figure 3B-D) were unaffected. Pre-treatment with RSM yielded similar results (supplemental Figure 3A-C). Shorter (6 h) pre-treatment was insufficient to affect *Retnla* expression (supplemental Figure 3D). Other cytokine genes including *Il10* and *Tnfa* were not affected (not shown).

Given the altered transcriptional responses following interruptions to choline metabolism, we next determined whether there were changes to IL-4R signaling.[27] In naïve macrophages, HC3 pre-treatment to block choline uptake increased basal Akt phosphorylation on S473 compared to vehicle treated (supplemental Figure 3E). In response to IL-4 stimulation, pAkt-S473 increased over 60 min in vehicle-treated BMDMs but was further elevated in HC3 pre-treated cells (Figure S3E). In addition, signaling to pSTAT6-Y641 after IL-4 stimulation, was significantly blunted by pre-treatment with HC3 or RSM (Figure 3E and supplemental Figure 3E). Together, this suggests that relatively acute disruptions of choline metabolism in macrophages could alter JAK1[13] and/or STAT6 signaling.

To further probe how limiting choline metabolism alters macrophage IL-4 polarization, we used CD38 and Egr2, which have been identified as effective discriminators of M[LPS] vs. M[IL-4], respectively[28]. Blocking choline uptake did not impair the induction of Egr2, nor did it promote CD38 expression in M[IL-4] (supplemental Figure 3F), despite Egr2 being induced in an IL-4/STAT6-dependent manner.[29] We next assessed the expression of the checkpoint ligands PD-L1 and PD-L2, which have also be used discriminate between M[LPS] and M[IL-4] polarization.[30] Inhibiting choline metabolism with either HC3 or RSM led to consistent PD-L1 up-regulation in M[0] and M[IL-4], but not in M[LPS] where expression was already maximal (Figure 3F). In contrast, inhibiting choline metabolism reduced PD-L2 expression in M[IL-4] (Figure 3F). Therefore, by limiting uptake and phosphorylation of choline, there were pointed changes to traditional IL-4-induced cytokines (e.g., *Retnla*) and a skewing toward a M[LPS]-like profile.

*Choline metabolism inhibition impairs macrophage function*

The secreted cytokine resistin-like molecule alpha (RELMα) is encoded by *Retnla* and has pleiotropic functions, including suppression of Th2 responses and promotion of wound healing.[31] In IL-4-polarized macrophages, blocking choline uptake significantly reduced intracellular RELMα levels (Figure 4A-B). Furthermore, to rule out off-target pharmacological effects, culture of M[IL-4] in choline-deficient media also curtailed intracellular RELMα to the same extent as HC3 and RSM (Figure 4A-B). Finally, we confirmed that secreted RELMα in M[IL-4]

conditioned media was significantly lower when choline uptake was inhibited (Figure 4C). Functionally, given that RELMα levels were dramatically reduced in response to altered choline uptake and metabolism, we sought to assess the *in vitro* wound healing capacity of macrophages. A "scratch wound" was created among 3T3-L1 fibroblasts grown to confluency and when exposed to conditioned media from HC-3-treated M[IL-4], we observed a significantly impaired rate of wound healing (Figure 4D).

*RSM-932a treatment* in vivo *reduces tissue-resident macrophage RELMα*

RELMα is strongly up-regulated upon IL-4 treatment *in vitro* but is also expressed endogenously in tissue-resident macrophages throughout the body, especially serosal cavity macrophages.[32,33] We next sought to pharmacologically block choline metabolism *in vivo* to interrogate whether this could mimic changes in IL-4 responses observed in cultured cells. Mice were dosed with RSM (3 mg/kg i.p.) every other day for seven days (Figure 5A). Previously, long-term RSM administration in preclinical tumour models resulted in significant reduction in tumour growth,[34] highlighting its low toxicity and therapeutic potential. Surprisingly, RSM treatment resulted in drastic remodelling of peritoneal exudate cell (PEC) populations (Figure 5B). Uniform manifold approximation and projection (UMAP) plots show a reduction in B cells, macrophages and eosinophils, and an increase in Gr-1$^{+}$ polymorphonuclear cells (PMNs) and monocytes. Furthermore, intracellular RELMα levels were significantly decreased in PEC macrophages taken from RSM-treated mice compared to vehicle control (Figure 5C, gating in supplemental Figure 4A). Moreover, expression of PD-L1 and PD-L2 was also significantly increased and reduced compared to vehicle-treated mice, respectively, which mirrored *in vitro* results. The suppressive effect of RSM on large (CD11b$^{high}$F4/80$^{+}$; LPM) and small peritoneal macrophages (CD11b$^{int}$F4/80$^{+}$; SPM) (Figure 5D-E), which contained high or moderate levels of intracellular RELMα was evident following just two doses, separated by 48 h (supplemental Figure 4B-C). RELMα is further found in white adipose tissue (WAT) and lung, and though previously thought to be an adipokine,[35] RELMα is mainly produced by WAT macrophages. Short-term RSM treatment increased WAT *Emr1* expression (supplemental Figure 4D) and matched the pattern of *in vitro* choline uptake or Chkα inhibited BMDMs with decreased *Retnla*, increased *Chil3*, and unchanged *Mrc1* (supplemental Figure 4E-G). Finally, we imaged ethyl cinnamate-cleared lungs[36] and found marked reduction in RELMα expression after RSM treatment (supplemental Figure 4H). Thus, *in vivo* inhibition of choline metabolism restructures endogenous tissue-resident macrophage phenotypes and supresses RELMα in multiple tissue compartments.

*Inhibiting choline metabolism with RSM improved measures of chemical-induced colitis*

The link between choline metabolism and RELMα was unexpected. To further probe the functional consequences of altering RELMα levels under pathophysiological conditions, we used dextran sodium sulfate (DSS) to chemically induce a state of colitis in female C57BL/6J mice over a 7-day protocol, where mice were given vehicle or RSM (3 mg/kg i.p.) bi-daily (supplemental Figure 5I). While there were no significant differences in body weight (supplemental Figure 5J), colon length was significantly longer and hemoccult was significantly lower in RSM-treated mice compared to control, respectively (supplemental Figure 5K-L). This is entirely consistent with previous reports where *Retnla*-deficient mice were protected against DSS-induced colitis.[37]

*Choline kinase inhibition does not affect helminth burden despite dramatic blunting of RELMα*

Our data suggest a role for choline metabolism in supporting IL-4-induced (Th2) responses *in vitro* and *in vivo*. To interrogate choline metabolism function in the physiologic setting of a Th2-skewed environment driven by helminth infection, we infected female mice with *Heligmosomoides polygyrus* (*Hp*), a parasitic nematode that colonizes the small intestine and drives protective M[IL-4]-like responses.[38] Mice were orally infected with *Hp* larvae and left for 8 days to allow parasites to develop into adults within the intestinal lumen, followed by treatment with RSM or vehicle every two days. Naïve mice were also treated with RSM at the same dose and interval to serve as controls for infection (Figure 6A). Treatment with RSM had modest effects on the weight of naïve or *Hp*-infected mice, with the trend of decreasing weight gain (shown in supplemental Figure 5A as a percent of initial weight). IL-4-polarized macrophages have been shown to play an important role in reducing helminth parasite burden;[39,40] yet, neither egg nor worm burden were affected following RSM treatment (Figure 6B-C). *Hp* infection significantly increased RELMα levels in the peritoneal fluid and serum; nevertheless, consistent with *in vitro* and *in vivo* observations, RELMα levels were significantly decreased with RSM treatment (Figure 6D-E). Furthermore, the presence of $CD206^+$ and $RELM\alpha^+$ cells in intestinal tissue, the primary site of infection, was also reduced (Figure 6F).

We next probed the effect of chronic RSM treatment in a vaccination model for *Hp* involving secondary infection (supplemental Figure 5B), where IL-4-polarized macrophages are critical for protection.[41] At week 8 post-infection, RSM treatment resulted in significantly increased fecal egg burden, suggestive of some deficiency in optimal immunity to the parasitic worm. However, there were no significant differences in egg burdens at the other timepoints, nor any differences in adult worm burden after secondary challenge (supplemental Figure 5C-D). Remarkably, consistent with the acute regiment, RSM treatment led to a significant drop in peritoneal and serum RELMα (supplemental Figure 5E-F), as well as down-regulated CD206 and upregulated CD86 expression in the intestinal cells of infected mice (supplemental Figure 5G). Together, this data indicates the importance of choline metabolism and choline kinase signaling in promoting M[IL-4] polarization and RELMα expression in intestinal helminth infection.

*Choline inhibition shifts peritoneal immunity and impairs M[IL-4] polarization to multiple helminth infections*

Intestinal *Hp* infection induces significant peritoneal cavity inflammation and macrophage M[IL-4] responses.[42] The striking RSM-induced changes in the peritoneal immune landscape of naïve mice was exacerbated during *Hp* infection (Figure 7A; supplemental Figure 6A). We detected more than a 10-fold increase in peritoneal cells compared to naïve mice and during infection, there was a significantly lower number total cells when mice were treated with RSM (Figure 7B). There was a substantial drop in eosinophils and B-1 cells in RSM-treated mice, accompanied by a rise in monocytes and neutrophils, both by frequencies and total cell numbers (Figure 7C-F). Peritoneal macrophages were also decreased by RSM treatment in both naïve and infected mice (Figure 7G). In addition, CD206 was significantly decreased in peritoneal macrophages, while both CD86 and PD-L1 were significantly increased, mimicking the suppressive effect of RSM on macrophage M[IL-4] polarization *in vitro* (Figure 7H-J). These results were directly recapitulated during chronic *Hp* infection and RSM treatment, where differences in resident peritoneal immune populations, as well as changes in macrophage and

intestinal expression of CD86 and CD206 (supplemental Figure 6B-G) in response to RSM were further aggravated.

Finally, to determine if blocking choline metabolism had broader impacts in other helminth infections, we treated mice with RSM following infection with *Nippostrongylus brasiliensis* (*Nb*), a natural rodent parasite that acutely infects the lung and small intestine, and drives macrophage M[IL-4] polarization and RELMα expression.[21,43] Treatment with RSM had no significant effects on parasite burden or bronchoalveolar macrophage responses (supplemental Figure 7A-F). However, in keeping with *in vitro* and *Hp* models, immunofluorescent staining of the naïve and infected lungs revealed that *Nb* induction of RELMα expression in the lung airway epithelial cells and parenchyma was completely abrogated with RSM treatment, while increased CD86 expression was observed (supplemental Figure 7G). Despite our previous observations that *Retnla*-deficient mice show lower parasite egg burden in *Nb* infection,[44] the complex phenotypic switch caused by inhibiting choline metabolism may mitigate the absence of RELMα for parasite burden outcomes. Taken together, these data support a major role for choline metabolism in sustaining RELMα expression and shaping the composition and phenotype of immune populations *in vivo*.

## Discussion

Upon activation, macrophages up-regulate choline metabolism to fuel PC synthesis. LPS and IL-4 both induce expansion of organellar membranes including ER, mitochondria, and endo-lysosomes,[45-48] in addition to a general enlargement of the cell itself.[49] Building on our understanding of macrophage choline metabolism during LPS polarization, we show here that stimulation of divergent signaling pathways (i.e., LPS-TLR4 vs. IL-4-JAK/STAT6), both lead to more choline taken into the cell via up-regulated CTL1, which facilitates increased flux through the PC synthetic pathway and more PC levels for membrane biogenesis. How phospholipid composition is affected by macrophage polarization has been addressed in studies using similar but still differential study designs. While the increased accumulation of PC in IL-4/IL13-polarized macrophages (RAW264.7 cells) was shown in a comprehensive assessment of phospholipid content after long term exposure to polarizing stimuli, this was not seen in human THP-1-derived macrophages,[50] nor were increases observed before 18 h.[46] Coupled with an increase in total PC content, we observed an increase in saturated and monounsaturated fatty acyl chains in PCs elevated in both M[IL-4] and M[LPS]. We and others have previously shown that M[LPS] up-regulate *de novo* lipogenesis to supply new FA for phospholipid synthesis.[4,10] There is now evidence to support a role for both exogenous FA uptake,[11,12] as well as *de novo* lipogenesis in M[IL-4].[51] Despite the potentially divergent sources of FA, differences in the side chain composition of choline-containing phospholipids between macrophage polarizations may fuel distinct lipid signaling pathways following phospholipase-specific processing.

A handful of studies have now interrogated the importance of choline metabolism in macrophage biology, though all have been in the context of LPS-induced polarization and inflammation.[4,5,9,52,53] Conversely, while macrophage IL-4 polarization is widely used *in vitro* and typically yields a reproducible response, how this might be affected by or might affect

choline metabolism remained unclear. By blocking choline uptake and/or subsequent metabolism, the transcriptional induction of *Mrc1*, *Chil3*, *Arg1* were not changed. However, limiting the availability of choline in the media, or pharmacologically blocking the uptake/phosphorylation of choline caused the targeted reduction in IL-4-induced *Retnla* expression and RELMα secretion. Signaling through STAT6 is essential for proper induction of Th2 cytokines and IL-4-induced RELMα expression.[54] In response to limiting choline availability and PC synthesis, STAT6 phosphorylation as a surrogate for IL-4R signaling efficacy, was decreased. However, while this supports the robust down-regulation of *Retnla*, similarly regulated transcripts such as *Chil3* were not affected or mildly increased. Curiously, *Chil3* has even been suggested to augment *Retnla* expression.[55] The mechanism(s) by which choline availability regulates *Retnla* are likely transcriptional; however, appear to be independent of IL-4 signaling (Figures 6 and S5). Interestingly, transient expression of *Retnla* was recently shown in nearly all tissue-resident macrophages and its induction in PEC macrophages was not IL-4ra-dependent.[56] Consistent with this, other studies report that RELMα is induced by signals other than Th2 cytokines, such as hypoxia or phagocytosis of apoptotic cells.[57,58] Our findings support the differential induction of canonical M[IL-4] genes, and identify choline metabolism as a specific inducer of *Retnla*. In our study, we found that Chkα inhibition resulted in major changes to PEC populations, akin to the macrophage disappearance reaction upon inflammatory stimuli,[59] pointing to a possible connection between macrophage tissue residence and choline metabolism. In addition, B cells in the peritoneum were drastically reduced, which corroborates previous observations demonstrating that RSM and another Chkα inhibitor (MN58B) dramatically lowered splenic B cell populations upon systemic delivery.[60] How this altered peritoneal immune profile may influence RELMα levels remains to be determined; however, since lung B cells express similar amounts of RELMα during *Nb* infection as alveolar macrophages,[61] the effect may not be exclusive to macrophages.

Macrophage-derived RELMα has been shown to promote profibrotic collagen cross-linking in fibroblasts,[62] while also contributing to pro-inflammatory processes in intestinal inflammation and infection.[37,63,64] Given that limiting choline metabolism in M[IL-4] markedly depleted RELMα levels and that *in vivo* RSM treatment recapitulated this effect, we reasoned that blocking choline metabolism during helminth infection may phenocopy models of RELMα deficiency, where enhanced resistance to parasites is observed.[43,44,65] Contrary to our hypothesis, RSM-mediated choline kinase inhibition had no impact on indices of parasite burden in any of the helminth models we assessed, despite profound reductions in local and systemic levels of RELMα (Figure 6; supplemental Figure 5 and 7). While the explanation for this remains unclear, there may be compensatory changes in RSM-treated mice, such as the altered immune profile, differential activation of macrophages, or direct effects of RSM on the pathogen that could confound the interpretation. The importance of macrophage-specific metabolism for M[IL-4] activation in the context of helminth infection has previously been shown. Inhibition of lysosomal lipolysis in *H. polygyrus*-infected mice reduced M[IL-4] polarization and RELMα expression, leading to increased parasite egg burden.[66] Similarly, our studies indicate that choline metabolism is also important in optimal M[IL-4] polarization in response to *H. polygyrus* infection, but with no effects on parasite burden. Future work could involve genetic and tissue-

specific models to directly address the relevance of macrophage choline metabolism in controlling helminth infections.

In addition to the striking effect on RELMα, we found the costimulatory checkpoint ligands PD-L1 and PD-L2 were coordinately regulated by choline metabolism, which is contrary to conventional IL-4-polarization. In tumour settings, nutrient availability may be heterogenous, especially for infiltrating immune cells, which can explain the wide range of PD-L1 positivity among tumour samples and the relatively poor response to anti-PD-1/PD-L1 immune-checkpoint inhibitor therapies.[67] Up-regulated choline metabolism is a recognized hallmark of certain cancers[68,69] and targeting Chkα can both inhibit cancer cell growth and render cell death-resistant cancers more susceptible to immunotherapy[70]. The level of PD-L1 induction and PD-L2 suppression upon blocking choline metabolism in the presence of IL-4 suggests a potential immunoregulatory role of choline metabolism that may represent an underappreciated therapeutic potential in cancer treatment.

Macrophages up-regulate choline uptake and incorporation in response to IL-4 stimulation. Reciprocally, when the availability of choline is compromised, normal IL-4 responses are affected. We used two pharmacological approaches to limit choline availability and nutrient deprivation in the media. These approaches carry numerous caveats, including dose, timing, route, and potential off-target effects; however, our *in vitro* pharmacological approach targeted distinct steps in the CDP-choline pathway. Separately, other fates of choline may be modified by or play a role in mediating the alteration of immune cell function. For instance, phosphocholine may post-translationally modify proteins,[71,72] and macrophages and other immune cells have been shown to produce acetylcholine.[73] Conversion of choline to betaine may also support osmoregulation[74] or contribute to histone methylation,[75] but these latter mechanisms require deeper investigation in immune contexts and remain speculative. Future work using genetic models to solidify the importance of choline uptake and subsequent metabolism are warranted.

In summary, we describe a critical role for choline metabolism in the mediating the full potential of macrophage M[IL-4] polarization. Moreover, systemic pharmacological inhibition of choline metabolism in mice closely mirrors the dramatic down-regulation of RELMα and PD-L2 and corresponding up-regulation of PD-L1 but fails to affect the pathology of intestinal or lung helminth infection models. This work also highlights that the inhibition of choline metabolism via RSM caused a dramatic shift in immune cell profile and potentially polarization, which may be therapeutically beneficial in other disease settings such as peritoneal metastases or fibrosis.

**Acknowledgements**

This work benefitted from data assembled by the ImmGen consortium. We thank Dr. Vera Tang and the Faculty of Medicine Flow Cytometry Core Facility, Dr. Chloë van Oostende-Triplet and the Cell Biology and Image Acquisition Core Facility, as well as the Animal Care and Veterinary Services at the University of Ottawa. Figures were created with BioRender.com.

**Funding**

This research was supported by a Discovery Grant from the Natural Sciences and Engineering Research Council of Canada (NSERC, RGPIN-2021-03503 to MDF), the Canadian Institutes of Health Research (CIHR, PJX-179853 to SALB) and National Institutes of Health (NIAID, R01AI153195 to MGN).

**Authorship**

Contribution: P.G., S.Y.K., T.K.T.S., L.M., M.K.K., M.I., I.A., S.A.S., K.D.M., J.R.C.N., D.W., C.P., C.O.D., and S.A.L.B. performed experiments and analyzed results. J.S.P. contributed reagents and equipment. P.G., S.Y.K., M.G.N., and M.D.F. designed the research, made the figures, and wrote the paper.

Conflict-of-interest disclosure: The authors declare no competing financial interests.

Co-Correspondence: Morgan D. Fullerton, Department of Biochemistry, Microbiology and Immunology, Faculty of Medicine, University of Ottawa, Ottawa, ON K1H 8M5; morgan.fullerton@uottawa.ca. Meera G. Nair, Division of Biomedical Sciences, University of California Riverside, Riverside, CA 92521; meera.nair@medsch.ucr.edu.

**Figure Legends**

**Figure 1 – IL-4 upregulates choline metabolism in macrophages.**

A) Relative expression of *Slc44a1* and *Slc44a2* transcripts in M[0] or M[IL-4], normalized to *Actb*. n=8 mice.

B) Expression by Western blot of CTL1 and CTL2 in M[0] or M[IL-4]. n=3, representative of 3 experiments. Unpaired t test (** $p < 0.01$).

C) Expression of CTL1 by surface flow cytometry after different IL-4 stimulation times. Representative of 2 experiments.

D) Uptake of $^{3}$H-choline over time in M[0] or M[IL-4]. n=2-3 per timepoint, representative of 3 experiments. Linear regression F test (**** $p < 0.0001$).

E) Incorporation of $^{3}$H-choline into phospholipids over time. n=5 per timepoint, representative of 3 experiments. Two-way ANOVA with Šídák's test for multiple comparisons (** $p < 0.01$, *** $p < 0.001$).

**Figure 2 – Phospholipid dynamics in polarized macrophages.**

A) Schematic of lipidomics analysis.

B) Total lipid content by individual phospholipid subclasses expressed as pmol per 1E6 cells and

C) heatmaps of the fold change of individual phospholipid species by subclass in M[0], M[IL-4], and M[LPS], relative to the average of M[0]. n=5 mice. LPCs identified as 1-acyl or 2-acyl LPCs were summed to account for in solution acyl-chain migration.

**Figure 3 – Choline uptake and phosphorylation is required for normal IL-4 signaling and M[IL-4] phenotype.**

A-D) Macrophages were treated with vehicle (DMSO) or HC3 (250 µM) for 24 h, washed, then treated with IL-4 (20 ng/mL) for 24 h. Relative expression of M[IL-4] hallmark genes *Retnla*, *Arg1*, *Mrc1*, *Chil3*, normalized to *Actb* and compared to M[0]. n=3, representative of 3-5 experiments. Unpaired t test (*** $p < 0.001$).

E) Macrophages were treated with vehicle (DMSO), HC3 (250 µM) or RSM-932a (5 µM) for 24 h, washed, then treated with IL-4 (20 ng/mL) for 15' and stained for intracellular pSTAT6 (Tyr641). n=3, representative of 3 experiments. Two-way ANOVA with Tukey's test for multiple comparisons (** $p < 0.01$, **** $p < 0.0001$).

F) Surface PD-L1 and PD-L2 expression in M[0], M[IL-4], or M[LPS], treated with vehicle, HC3 (250 µM) or RSM-932a (5 µM). n=2, representative of 3 experiments.

**Figure 4 – Inhibiting choline uptake impairs RELMα expression and secretion and reduces wound healing process of fibroblasts exposed to macrophage conditioned media.**

A-B) Macrophages were treated with vehicle (DMSO) or HC3 (250 µM) for 24 h, washed, then treated with IL-4 (20 ng/mL) for 24 h in complete or choline-deficient (ΔCho) media. B) Quantification of intracellular RELMα staining in live $F480^+$ macrophages. n=3, representative of >4 experiments. One-way ANOVA with Tukey's test for multiple comparisons (* $p < 0.05$, ** $p < 0.01$).

C) Macrophages were treated with vehicle (DMSO), HC3 (250 µM), or RSM-932a (5 µM) for 24 h, washed, then treated with IL-4 (20 ng/mL) for 24 h. Detection of supernatant RELMα by ELISA. n=5 (vehicle, HC3, IL-4) or n=2 (RSM). Unpaired t test (** $p < 0.01$).

D) Macrophages were treated with vehicle (DMSO) or HC3 (250 µM) for 24 h, washed, then treated with IL-4 (20 ng/mL) for 24 h and conditioned media was collected. Confluent 3T3-L1 fibroblast monolayers were scratched, and media was replaced with macrophage conditioned media. Images of wound healing over time, quantified by wound density. n=3, representative of 2 experiments. Sum-of-squares F test of non-linear fit of growth curves (**** $p < 0.0001$).

**Figure 5 – *In vivo* choline kinase inhibition remodels peritoneal cell populations and impairs RELMα expression**

A) Schematic of 7-day *in vivo* choline kinase inhibition. Mice were treated intraperitoneally with vehicle (40% DMSO in PBS) or RSM-932a (3 mg/kg) every other day for 6 days and sacrificed on day 7.

B) UMAP of peritoneal cell populations. n=9-10, N=2.

C) Intracellular RELMα expression in live $CD11b^{hi}Ly6C^{+}$ and $CD11b^{int}Ly6C^{-}$ peritoneal cells. Two-way ANOVA with Šídák's test for multiple comparisons (* $p < 0.05$, **** $p < 0.001$).

D-E) PD-L1 or PD-L2 expression (gMFI) in live $CD11b^{+}F480^{+}$ and $CD11b^{+}F480^{-}$ peritoneal cells. Two-way ANOVA with Šídák's test for multiple comparisons (* $p < 0.05$, ** $p < 0.01$, *** $p < 0.001$).

**Figure 6 - *In vivo* choline kinase inhibition during primary intestinal helminth infection impairs systemic and intestinal RELMα and intestinal macrophage alternative activation**

A) Schematic of primary infection with 200 *H. polygyrus* (*Hp*) L3 larvae through oral gavage. Mice were treated intraperitoneally with vehicle (40% DMSO in PBS) or RSM-932a (3 mg/kg) every other day for 8 days starting on day 8 and sacrificed on day 17.

B-C) Eggs in feces were counted at multiple time points after infection, and C) adult worms were isolated from the small intestine and enumerated on the day of sacrifice. Values represent means ± SEM (n = 3-5 mice per group), representative of 3 experiments. Two-way ANOVA with Šídák's test for multiple comparisons and unpaired t test (ns).

D-E) Detection of serum and E) peritoneal fluid RELMα by ELISA in naïve and *H. polygyrus*-infected mice. n=3-5 per group. Two-way ANOVA with Šídák's test for multiple comparisons (* $p < 0.05$, *** $p < 0.001$ for differences between treatment and $^{\#\#}$ $p < 0.01$ for differences between naïve and infection).

F) Immunofluorescent staining of intestinal tissue for CD206 and RELMα against DAPI counterstain. Scale bar 50 µm. Quantification of $CD206^{+}$ or $RELM\alpha^{+}$ per $DAPI^{+}$ cell. n=6. Unpaired t test (* $p < 0.05$).

**Figure 7 – *In vivo* choline kinase inhibition in naïve mice and primary infection alters peritoneal cell populations and macrophage alternative activation**

A) UMAP plots of peritoneal cells (PECs) from naïve and *H. polygyrus*-infected mice treated with vehicle or RSM-932a. See Supplemental Figure 6A for population gating.

B-G) Enumeration of B) total PECs, C) eosinophils, D) monocytes, E) B-1 cells, F) neutrophils, G) peritoneal macrophages among live PECs. n=3-4 (naïve) or n=5 (infected). Two-way ANOVA with Šídák's test for multiple comparisons (* $p < 0.05$, ** $p < 0.01$, *** $p < 0.001$, **** $p < 0.0001$).

H-I) CD206, I) CD86, or J) PD-L1 expression (gMFI) on peritoneal macrophages. n=3-4 (naïve) or n=5 (infected). Two-way ANOVA with Šídák's test for multiple comparisons (* $p < 0.05$).

## References

1. Ginhoux F, Guilliams M. Tissue-Resident Macrophage Ontogeny and Homeostasis. *Immunity*. 2016;44(3):439-449.
2. Verberk SGS, de Goede KE, Gorki FS, van Dierendonck XAMH, Argüello RJ, Van den Bossche J. An integrated toolbox to profile macrophage immunometabolism. *Cell Reports Methods*. 2022;2(4):100192.
3. Gibellini F, Smith TK. The Kennedy pathway--De novo synthesis of phosphatidylethanolamine and phosphatidylcholine. *IUBMB Life*. 2010;62(6):414-428.
4. Snider SA, Margison KD, Ghorbani P, et al. Choline transport links macrophage phospholipid metabolism and inflammation. *J Biol Chem*. 2018;293(29):11600-11611.
5. Sanchez-Lopez E, Zhong Z, Stubelius A, et al. Choline Uptake and Metabolism Modulate Macrophage IL-1beta and IL-18 Production. *Cell Metab*. 2019;29(6):1350-1362 e1357.
6. Kennedy EP, Weiss SB. The function of cytidine coenzymes in the biosynthesis of phospholipides. *J Biol Chem*. 1956;222(1):193-214.
7. Jackowski S. Coordination of membrane phospholipid synthesis with the cell cycle. *J Biol Chem*. 1994;269(5):3858-3867.
8. Zhang D, Tang W, Yao PM, et al. Macrophages deficient in CTP:Phosphocholine cytidylyltransferase-alpha are viable under normal culture conditions but are highly susceptible to free cholesterol-induced death. Molecular genetic evidence that the induction of phosphatidylcholine biosynthesis in free cholesterol-loaded macrophages is an adaptive response. *J Biol Chem*. 2000;275(45):35368-35376.
9. Tian Y, Pate C, Andreolotti A, et al. Cytokine secretion requires phosphatidylcholine synthesis. *J Cell Biol*. 2008;181(6):945-957.
10. Hsieh WY, Zhou QD, York AG, et al. Toll-Like Receptors Induce Signal-Specific Reprogramming of the Macrophage Lipidome. *Cell Metab*. 2020;32(1):128-143 e125.
11. Koganesawa M, Yamaguchi M, Samuchiwal SK, Balestrieri B. Lipid Profile of Activated Macrophages and Contribution of Group V Phospholipase A2. *Biomolecules*. 2020;11(1).
12. Morgan PK, Huynh K, Pernes G, et al. Macrophage polarization state affects lipid composition and the channeling of exogenous fatty acids into endogenous lipid pools. *J Biol Chem*. 2021;297(6):101341.
13. Keegan AD, Zamorano J, Keselman A, Heller NM. IL-4 and IL-13 Receptor Signaling From 4PS to Insulin Receptor Substrate 2: There and Back Again, a Historical View. *Front Immunol*. 2018;9:1037.
14. Lechner A, Bohnacker S, Esser-von Bieren J. Macrophage regulation & function in helminth infection. *Semin Immunol*. 2021;53:101526.
15. Fullerton MD, Ford RJ, McGregor CP, et al. Salicylate improves macrophage cholesterol homeostasis via activation of Ampk. *J Lipid Res*. 2015;56(5):1025-1033.
16. Galic S, Fullerton MD, Schertzer JD, et al. Hematopoietic AMPK beta1 reduces mouse adipose tissue macrophage inflammation and insulin resistance in obesity. *J Clin Invest*. 2011;121(12):4903-4915.
17. Bligh EG, Dyer WJ. A rapid method of total lipid extraction and purification. *Can J Biochem Physiol*. 1959;37(8):911-917.
18. Xu H, Valenzuela N, Fai S, Figeys D, Bennett SA. Targeted lipidomics - advances in profiling lysophosphocholine and platelet-activating factor second messengers. *FEBS J*. 2013;280(22):5652-5667.

19. Chitpin JG, Surendra A, Nguyen TT, et al. BATL: Bayesian annotations for targeted lipidomics. *Bioinformatics*. 2021.
20. Livak KJ, Schmittgen TD. Analysis of relative gene expression data using real-time quantitative PCR and the 2(-Delta Delta C(T)) Method. *Methods*. 2001;25(4):402-408.
21. Chen G, Wang SH, Jang JC, Odegaard JI, Nair MG. Comparison of RELMα and RELMβ Single- and Double-Gene-Deficient Mice Reveals that RELMα Expression Dictates Inflammation and Worm Expulsion in Hookworm Infection. *Infect Immun*. 2016;84(4):1100-1111.
22. Johnston CJ, Robertson E, Harcus Y, et al. Cultivation of Heligmosomoides polygyrus: an immunomodulatory nematode parasite and its secreted products. *J Vis Exp*. 2015(98):e52412.
23. Camberis M, Le Gros G, Urban J. Animal model of Nippostrongylus brasiliensis and Heligmosomoides polygyrus. *Curr Protoc Immunol*. 2003;Chapter 19:Unit 19.12.
24. Bankhead P, Loughrey MB, Fernandez JA, et al. QuPath: Open source software for digital pathology image analysis. *Sci Rep*. 2017;7(1):16878.
25. Hwang WC, Seo SH, Kang M, et al. PLD1 and PLD2 differentially regulate the balance of macrophage polarization in inflammation and tissue injury. *J Cell Physiol*. 2021;236(7):5193-5211.
26. Schueler FW. A new group of respiratory paralyzants. I. The "hemicholiniums". *J Pharmacol Exp Ther*. 1955;115(2):127-143.
27. Junttila IS. Tuning the Cytokine Responses: An Update on Interleukin (IL)-4 and IL-13 Receptor Complexes. *Front Immunol*. 2018;9:888.
28. Jablonski KA, Amici SA, Webb LM, et al. Novel Markers to Delineate Murine M1 and M2 Macrophages. *PLoS One*. 2015;10(12):e0145342.
29. Daniel B, Czimmerer Z, Halasz L, et al. The transcription factor EGR2 is the molecular linchpin connecting STAT6 activation to the late, stable epigenomic program of alternative macrophage polarization. *Genes Dev*. 2020;34(21-22):1474-1492.
30. Loke Pn, Allison JP. PD-L1 and PD-L2 are differentially regulated by Th1 and Th2 cells. *Proceedings of the National Academy of Sciences*. 2003;100(9):5336-5341.
31. Pine GM, Batugedara HM, Nair MG. Here, there and everywhere: Resistin-like molecules in infection, inflammation, and metabolic disorders. *Cytokine*. 2018;110:442-451.
32. Summers KM, Bush SJ, Hume DA. Network analysis of transcriptomic diversity amongst resident tissue macrophages and dendritic cells in the mouse mononuclear phagocyte system. *PLoS Biol*. 2020;18(10):e3000859.
33. Bain CC, Hawley CA, Garner H, et al. Long-lived self-renewing bone marrow-derived macrophages displace embryo-derived cells to inhabit adult serous cavities. *Nat Commun*. 2016;7:ncomms11852.
34. Lacal JC, Campos JM. Preclinical characterization of RSM-932A, a novel anticancer drug targeting the human choline kinase alpha, an enzyme involved in increased lipid metabolism of cancer cells. *Mol Cancer Ther*. 2015;14(1):31-39.
35. Lee MR, Lim CJ, Lee YH, et al. The adipokine Retnla modulates cholesterol homeostasis in hyperlipidemic mice. *Nat Commun*. 2014;5:4410.
36. Masselink W, Reumann D, Murawala P, et al. Broad applicability of a streamlined ethyl cinnamate-based clearing procedure. *Development*. 2019;146(3).
37. Munitz A, Waddell A, Seidu L, et al. Resistin-like molecule alpha enhances myeloid cell activation and promotes colitis. *J Allergy Clin Immunol*. 2008;122(6):1200-1207 e1201.

38. Bouchery T, Volpe B, Shah K, et al. The Study of Host Immune Responses Elicited by the Model Murine Hookworms Nippostrongylus brasiliensis and Heligmosomoides polygyrus. *Curr Protoc Mouse Biol*. 2017;7(4):236-286.
39. Chen F, Wu W, Millman A, et al. Neutrophils prime a long-lived effector macrophage phenotype that mediates accelerated helminth expulsion. *Nat Immunol*. 2014;15(10):938-946.
40. Obata-Ninomiya K, Ishiwata K, Tsutsui H, et al. The skin is an important bulwark of acquired immunity against intestinal helminths. *J Exp Med*. 2013;210(12):2583-2595.
41. Anthony RM, Urban JF, Alem F, et al. Memory T(H)2 cells induce alternatively activated macrophages to mediate protection against nematode parasites. *Nat Med*. 2006;12(8):955-960.
42. Filbey KJ, Varyani F, Harcus Y, et al. Macrophage Migration Inhibitory Factor (MIF) Is Essential for Type 2 Effector Cell Immunity to an Intestinal Helminth Parasite. *Front Immunol*. 2019;10:2375.
43. Batugedara HM, Li J, Chen G, et al. Hematopoietic cell-derived RELMalpha regulates hookworm immunity through effects on macrophages. *J Leukoc Biol*. 2018;104(4):855-869.
44. Chen G, Wang SH, Jang JC, Odegaard JI, Nair MG. Comparison of RELMalpha and RELMbeta Single- and Double-Gene-Deficient Mice Reveals that RELMalpha Expression Dictates Inflammation and Worm Expulsion in Hookworm Infection. *Infect Immun*. 2016;84(4):1100-1111.
45. Hipolito VEB, Diaz JA, Tandoc KV, et al. Enhanced translation expands the endo-lysosome size and promotes antigen presentation during phagocyte activation. *PLOS Biology*. 2019;17(12):e3000535.
46. Castoldi A, Monteiro LB, van Teijlingen Bakker N, et al. Triacylglycerol synthesis enhances macrophage inflammatory function. *Nature Communications*. 2020;11(1):4107.
47. Vats D, Mukundan L, Odegaard JI, et al. Oxidative metabolism and PGC-1beta attenuate macrophage-mediated inflammation. *Cell Metab*. 2006;4(1):13-24.
48. Willenborg S, Sanin DE, Jais A, et al. Mitochondrial metabolism coordinates stage-specific repair processes in macrophages during wound healing. *Cell Metab*. 2021;33(12):2398-2414 e2399.
49. Ying W, Cheruku PS, Bazer FW, Safe SH, Zhou B. Investigation of macrophage polarization using bone marrow derived macrophages. *J Vis Exp*. 2013(76).
50. Zhang C, Wang Y, Wang F, et al. Quantitative profiling of glycerophospholipids during mouse and human macrophage differentiation using targeted mass spectrometry. *Sci Rep*. 2017;7(1):412.
51. Bidault G, Virtue S, Petkevicius K, et al. SREBP1-induced fatty acid synthesis depletes macrophages antioxidant defences to promote their alternative activation. *Nat Metab*. 2021;3(9):1150-1162.
52. Petkevicius K, Virtue S, Bidault G, et al. Accelerated phosphatidylcholine turnover in macrophages promotes adipose tissue inflammation in obesity. *Elife*. 2019;8.
53. Trajkovic-Bodennec S, Bodennec J, Futerman AH. Phosphatidylcholine metabolism is altered in a monocyte-derived macrophage model of Gaucher disease but not in lymphocytes. *Blood Cells Mol Dis*. 2004;33(1):77-82.
54. Stutz AM, Pickart LA, Trifilieff A, Baumruker T, Prieschl-Strassmayr E, Woisetschlager M. The Th2 cell cytokines IL-4 and IL-13 regulate found in inflammatory zone 1/resistin-like molecule alpha gene expression by a STAT6 and CCAAT/enhancer-binding protein-dependent mechanism. *J Immunol*. 2003;170(4):1789-1796.

55. Sutherland TE, Ruckerl D, Logan N, Duncan S, Wynn TA, Allen JE. Ym1 induces RELMalpha and rescues IL-4Ralpha deficiency in lung repair during nematode infection. *PLoS Pathog*. 2018;14(11):e1007423.
56. Sanin DE, Ge Y, Marinkovic E, et al. A common framework of monocyte-derived macrophage activation. *Sci Immunol*. 2022;7(70):eabl7482.
57. Bosurgi L, Cao YG, Cabeza-Cabrerizo M, et al. Macrophage function in tissue repair and remodeling requires IL-4 or IL-13 with apoptotic cells. *Science*. 2017;356(6342):1072-1076.
58. Lin Q, Fan C, Skinner JT, et al. RELMalpha Licenses Macrophages for Damage-Associated Molecular Pattern Activation to Instigate Pulmonary Vascular Remodeling. *J Immunol*. 2019;203(11):2862-2871.
59. Zhang N, Czepielewski RS, Jarjour NN, et al. Expression of factor V by resident macrophages boosts host defense in the peritoneal cavity. *J Exp Med*. 2019;216(6):1291-1300.
60. Gokhale S, Lu W, Zhu S, et al. Elevated Choline Kinase alpha-Mediated Choline Metabolism Supports the Prolonged Survival of TRAF3-Deficient B Lymphocytes. *J Immunol*. 2020;204(2):459-471.
61. Chen F, Wu W, Jin L, et al. B Cells Produce the Tissue-Protective Protein RELMalpha during Helminth Infection, which Inhibits IL-17 Expression and Limits Emphysema. *Cell Rep*. 2018;25(10):2775-2783 e2773.
62. Knipper JA, Willenborg S, Brinckmann J, et al. Interleukin-4 Receptor alpha Signaling in Myeloid Cells Controls Collagen Fibril Assembly in Skin Repair. *Immunity*. 2015;43(4):803-816.
63. Munitz A, Seidu L, Cole ET, Ahrens R, Hogan SP, Rothenberg ME. Resistin-like molecule alpha decreases glucose tolerance during intestinal inflammation. *J Immunol*. 2009;182(4):2357-2363.
64. Osborne LC, Joyce KL, Alenghat T, et al. Resistin-like molecule alpha promotes pathogenic Th17 cell responses and bacterial-induced intestinal inflammation. *J Immunol*. 2013;190(5):2292-2300.
65. Pesce JT, Ramalingam TR, Wilson MS, et al. Retnla (relmalpha/fizz1) suppresses helminth-induced Th2-type immunity. *PLoS Pathog*. 2009;5(4):e1000393.
66. Huang SC, Everts B, Ivanova Y, et al. Cell-intrinsic lysosomal lipolysis is essential for alternative activation of macrophages. *Nat Immunol*. 2014;15(9):846-855.
67. Doroshow DB, Bhalla S, Beasley MB, et al. PD-L1 as a biomarker of response to immune-checkpoint inhibitors. *Nat Rev Clin Oncol*. 2021;18(6):345-362.
68. Glunde K, Bhujwalla ZM, Ronen SM. Choline metabolism in malignant transformation. *Nat Rev Cancer*. 2011;11(12):835-848.
69. Pavlova NN, Thompson CB. The Emerging Hallmarks of Cancer Metabolism. *Cell Metab*. 2016;23(1):27-47.
70. Mariotto E, Viola G, Ronca R, et al. Choline Kinase Alpha Inhibition by EB-3D Triggers Cellular Senescence, Reduces Tumor Growth and Metastatic Dissemination in Breast Cancer. *Cancers (Basel)*. 2018;10(10).
71. Lovell TM, Woods RJ, Butlin DJ, et al. Identification of a novel mammalian post-translational modification, phosphocholine, on placental secretory polypeptides. *J Mol Endocrinol*. 2007;39(3):189-198.
72. Dixit A, Jose GP, Shanbhag C, Tagad N, Kalia J. Metabolic Labeling-Based Chemoproteomics Establishes Choline Metabolites as Protein Function Modulators. *ACS Chem Biol*. 2022;17(8):2272-2283.

73. Fujii T, Mashimo M, Moriwaki Y, et al. Expression and Function of the Cholinergic System in Immune Cells. *Front Immunol*. 2017;8:1085.
74. Tscherner AK, Macaulay AD, Ortman CS, Baltz JM. Initiation of cell volume regulation and unique cell volume regulatory mechanisms in mammalian oocytes and embryos. *J Cell Physiol*. 2021;236(10):7117-7133.
75. Bekdash RA. Early Life Nutrition and Mental Health: The Role of DNA Methylation. *Nutrients*. 2021;13(9).

# Figure 1

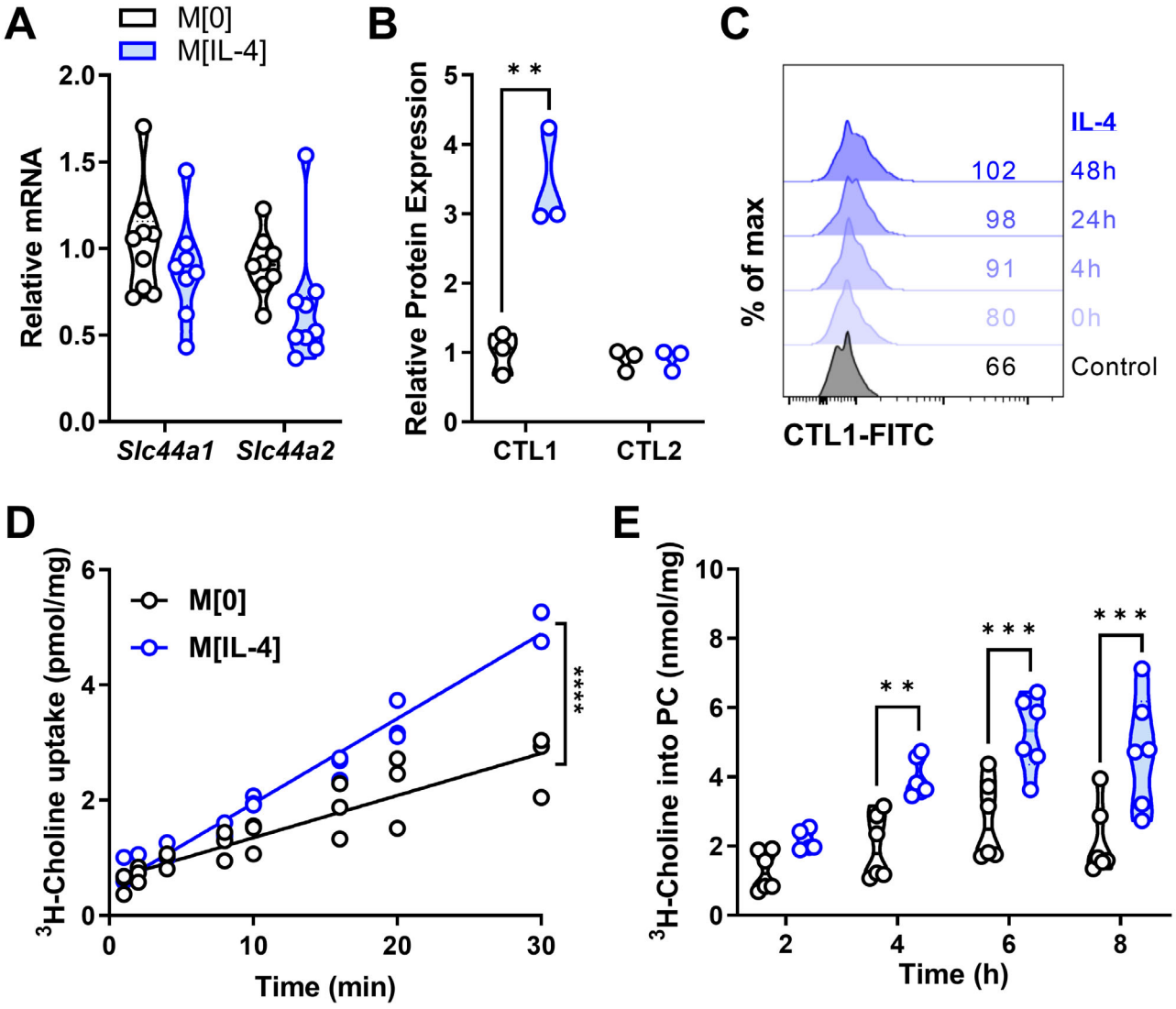
A
M[0]
M[IL-4]
Relative mRNA
2.0
1.5
1.0
0.5
0.0
Slc44a1
Slc44a2
B
Relative Protein Expression
5
4
3
2
1
0
* *
CTL1
CTL2
C
% of max
IL-4
102
48h
98
24h
91
4h
80
0h
66
Control
CTL1-FITC
D
M[0]
M[IL-4]
$^3$H-Choline uptake (pmol/mg)
6
4
2
0
****
0
10
20
30
Time (min)
E
$^3$H-Choline into PC (nmol/mg)
10
8
6
4
2
0
* *
* * *
* * *
2
4
6
8
Time (h)

## Figure 2

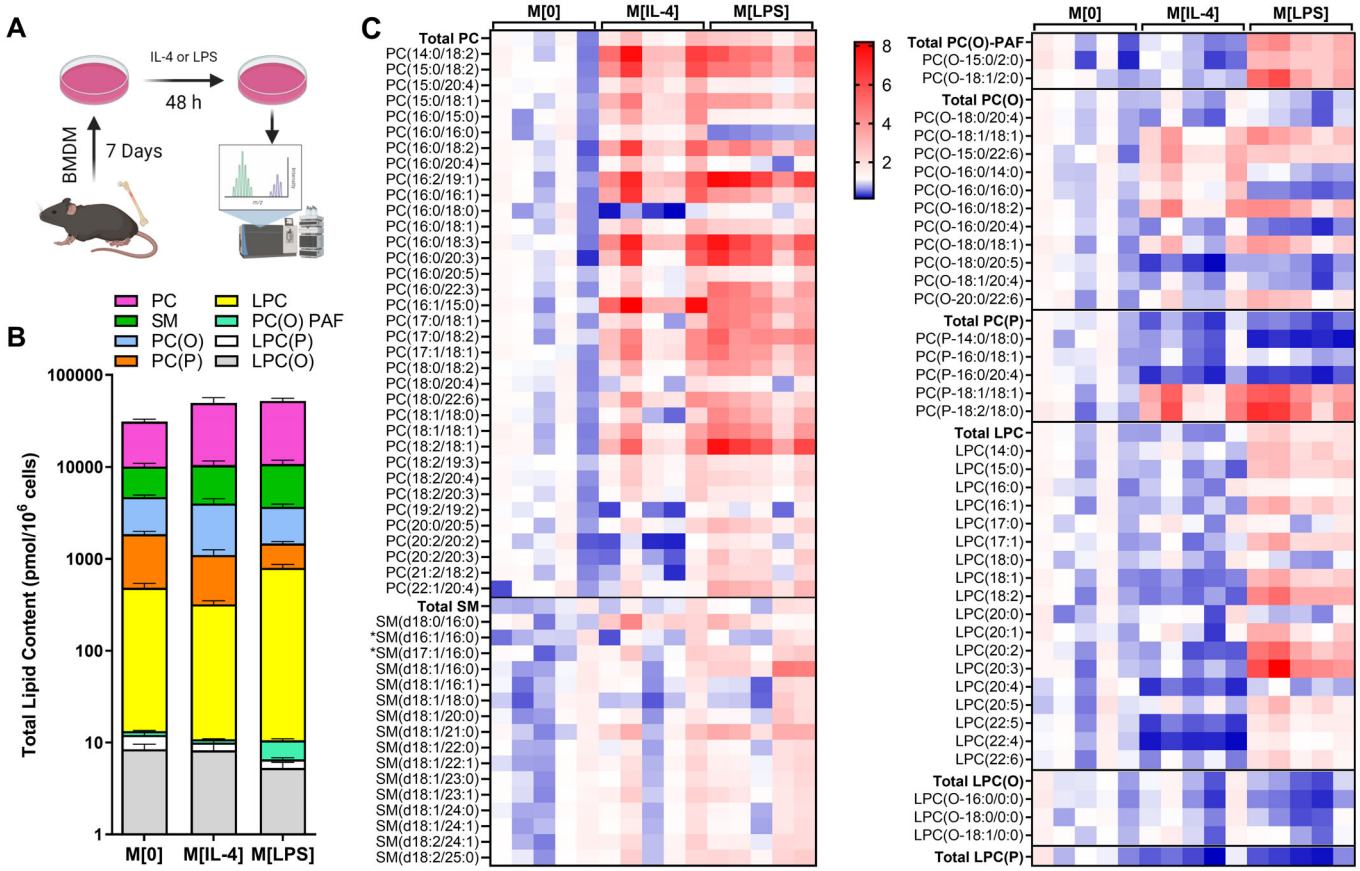
A
IL-4 or LPS
48 h
BMDM
7 Days
B
PC
SM
PC(O)
PC(P)
LPC
PC(O) PAF
LPC(P)
LPC(O)
Total Lipid Content (pmol/10^6 cells)
100000
10000
1000
100
10
1
M[0]
M[IL-4]
M[LPS]
C
M[0]
M[IL-4]
M[LPS]
Total PC
PC(14:0/18:2)
PC(15:0/18:2)
PC(15:0/20:4)
PC(15:0/18:1)
PC(16:0/15:0)
PC(16:0/16:0)
PC(16:0/18:2)
PC(16:0/20:4)
PC(16:2/19:1)
PC(16:0/16:1)
PC(16:0/18:0)
PC(16:0/18:1)
PC(16:0/18:3)
PC(16:0/20:3)
PC(16:0/20:5)
PC(16:0/22:3)
PC(16:1/15:0)
PC(17:0/18:1)
PC(17:0/18:2)
PC(17:1/18:1)
PC(18:0/18:2)
PC(18:0/20:4)
PC(18:0/22:6)
PC(18:1/18:0)
PC(18:1/18:1)
PC(18:2/18:1)
PC(18:2/19:3)
PC(18:2/20:4)
PC(18:2/20:3)
PC(19:2/19:2)
PC(20:0/20:5)
PC(20:2/20:2)
PC(20:2/20:3)
PC(21:2/18:2)
PC(22:1/20:4)
Total SM
SM(d18:0/16:0)
*SM(d16:1/16:0)
*SM(d17:1/16:0)
SM(d18:1/16:0)
SM(d18:1/16:1)
SM(d18:1/18:0)
SM(d18:1/20:0)
SM(d18:1/21:0)
SM(d18:1/22:0)
SM(d18:1/22:1)
SM(d18:1/23:0)
SM(d18:1/23:1)
SM(d18:1/24:0)
SM(d18:1/24:1)
SM(d18:2/24:1)
SM(d18:2/25:0)
8
6
4
2
M[0]
M[IL-4]
M[LPS]
Total PC(O)-PAF
PC(O-15:0/2:0)
PC(O-18:1/2:0)
Total PC(O)
PC(O-18:0/20:4)
PC(O-18:1/18:1)
PC(O-15:0/22:6)
PC(O-16:0/14:0)
PC(O-16:0/16:0)
PC(O-16:0/18:2)
PC(O-16:0/20:4)
PC(O-18:0/18:1)
PC(O-18:0/20:5)
PC(O-18:1/20:4)
PC(O-20:0/22:6)
Total PC(P)
PC(P-14:0/18:0)
PC(P-16:0/18:1)
PC(P-16:0/20:4)
PC(P-18:1/18:1)
PC(P-18:2/18:0)
Total LPC
LPC(14:0)
LPC(15:0)
LPC(16:0)
LPC(16:1)
LPC(17:0)
LPC(17:1)
LPC(18:0)
LPC(18:1)
LPC(18:2)
LPC(20:0)
LPC(20:1)
LPC(20:2)
LPC(20:3)
LPC(20:4)
LPC(20:5)
LPC(22:5)
LPC(22:4)
LPC(22:6)
Total LPC(O)
LPC(O-16:0/0:0)
LPC(O-18:0/0:0)
LPC(O-18:1/0:0)
Total LPC(P)

## Figure 3

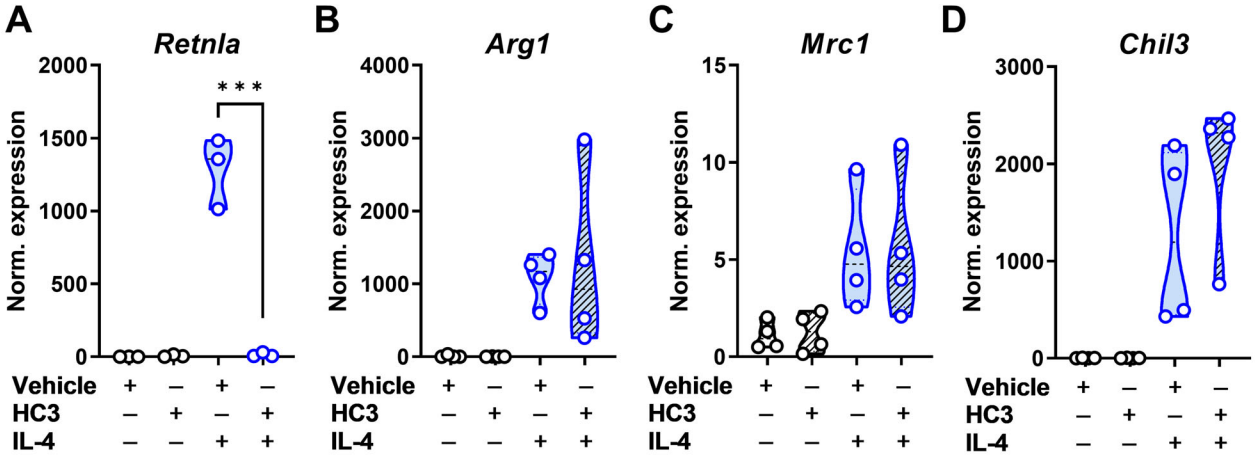
A
Retnla
B
Arg1
C
Mrc1
D
Chil3
Norm. expression
Vehicle
HC3
IL-4
* * *

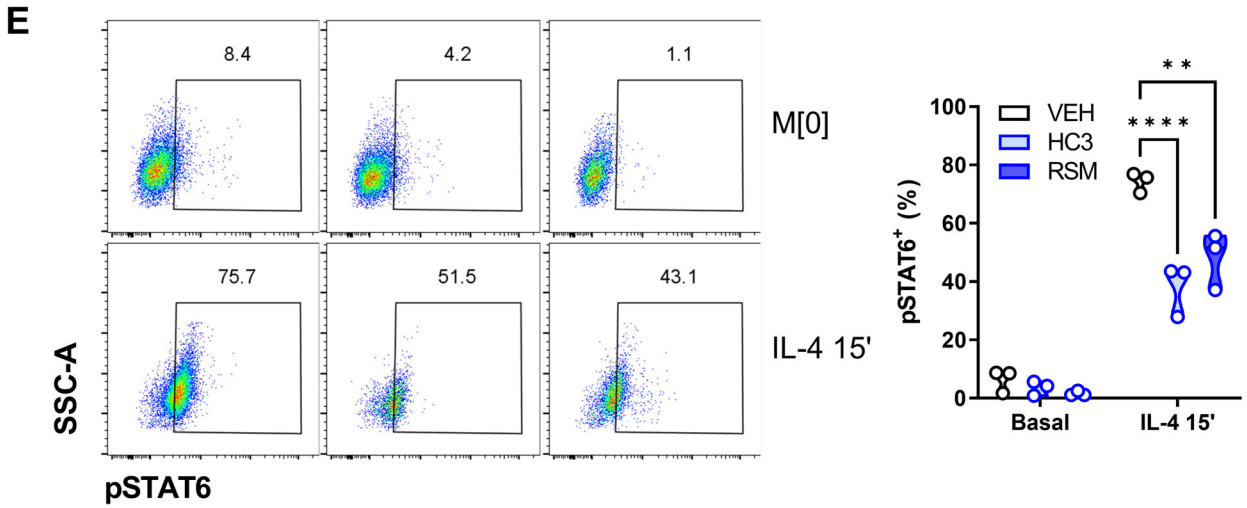
E
8.4
4.2
1.1
M[0]
75.7
51.5
43.1
IL-4 15'
SSC-A
pSTAT6
VEH
HC3
RSM
pSTAT6+ (%)
Basal
IL-4 15'
* *
* * * *

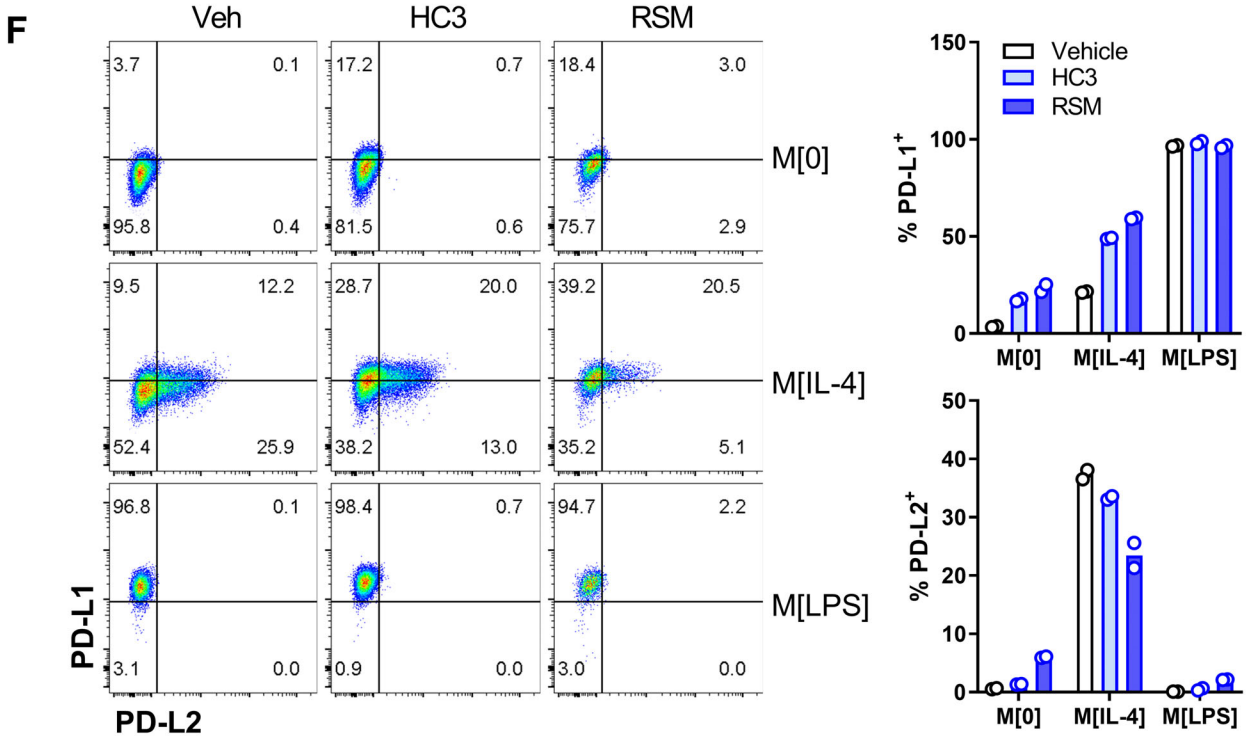
F
Veh
HC3
RSM
M[0]
M[IL-4]
M[LPS]
PD-L1
PD-L2
Vehicle
% PD-L1+
% PD-L2+

## Figure 4

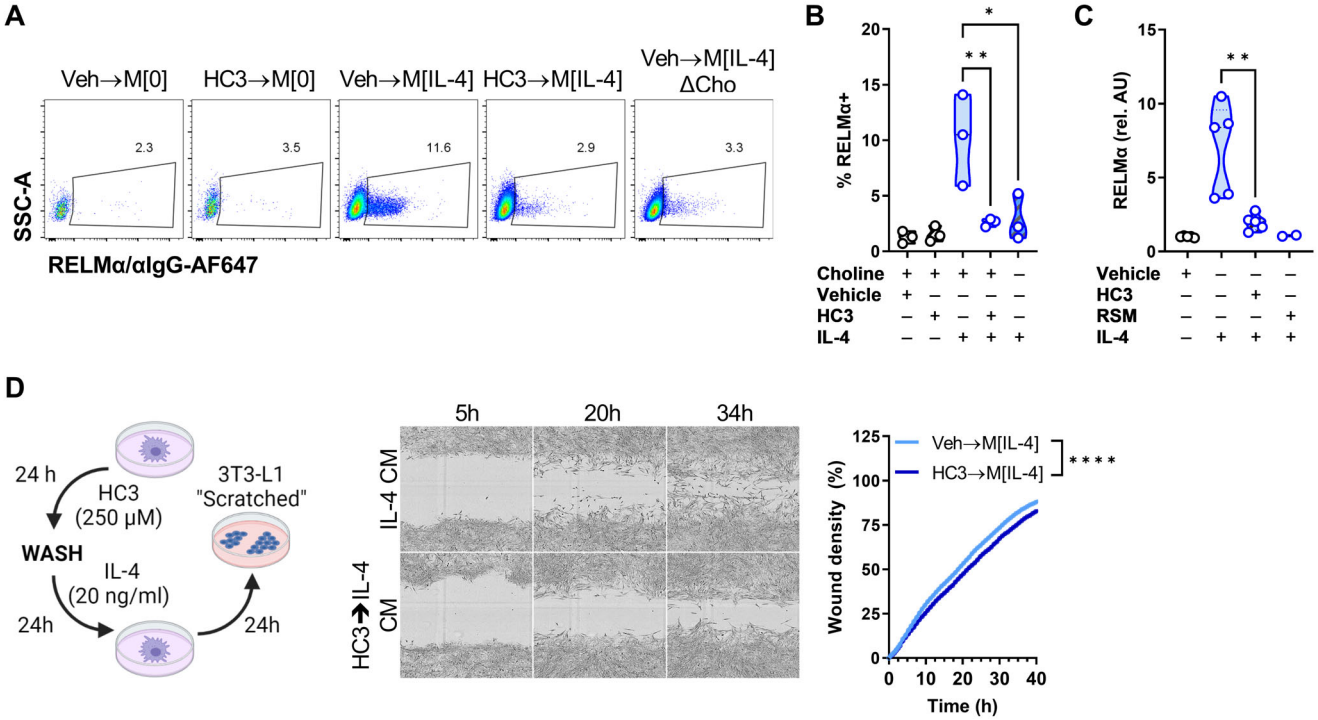
A
Veh→M[0]
HC3→M[0]
Veh→M[IL-4]
HC3→M[IL-4]
Veh→M[IL-4] ΔCho
2.3
3.5
11.6
2.9
3.3
SSC-A
RELMα/αIgG-AF647
B
% RELMα+
Choline
Vehicle
HC3
IL-4
C
RELMα (rel. AU)
Vehicle
HC3
RSM
IL-4
D
24 h
HC3 (250 μM)
WASH
IL-4 (20 ng/ml)
24h
3T3-L1 "Scratched"
24h
5h
20h
34h
IL-4 CM
HC3➔IL-4 CM
Veh→M[IL-4]
HC3→M[IL-4]
Wound density (%)
Time (h)

# Figure 5

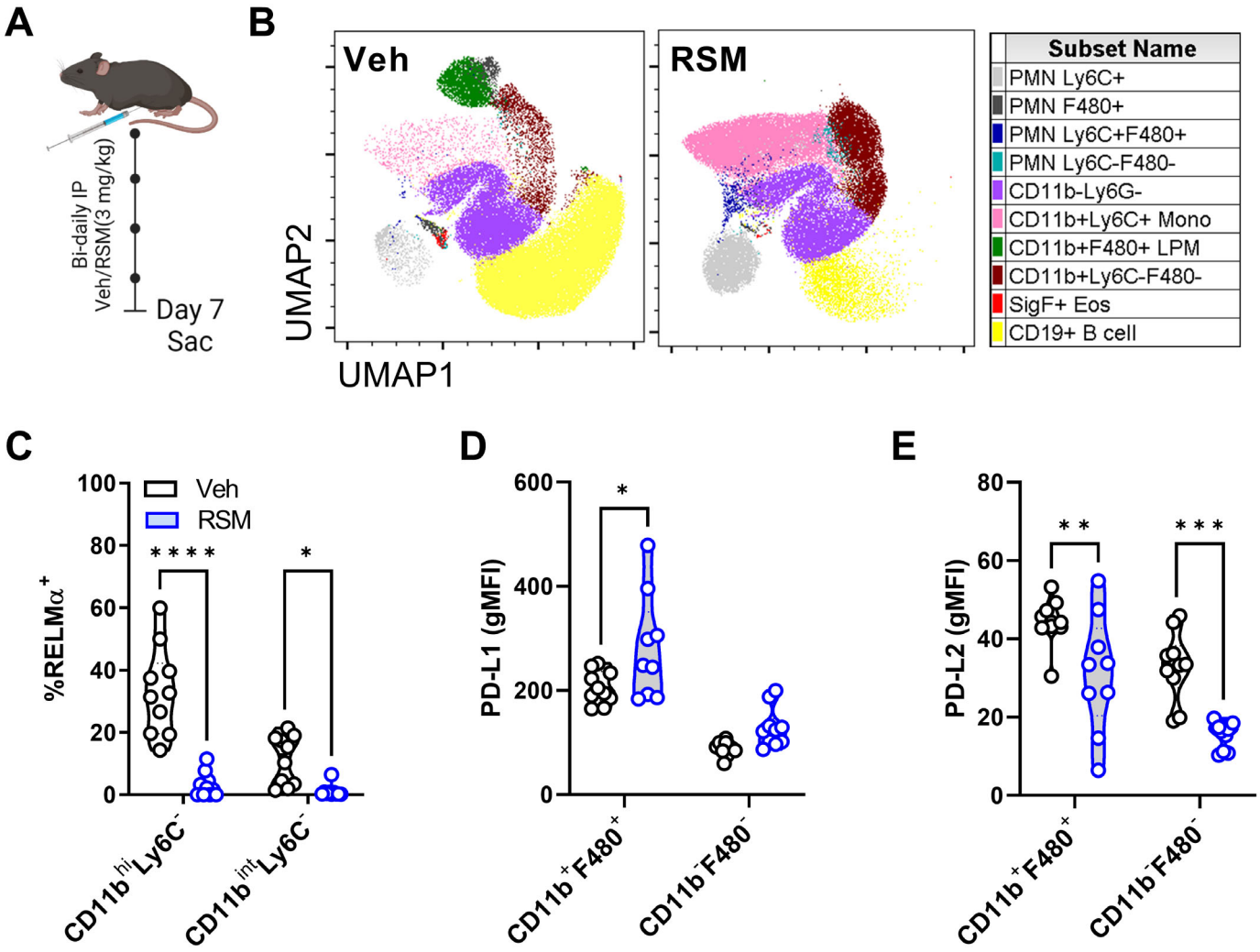
A
Bi-daily IP
Veh/RSM(3 mg/kg)
Day 7
Sac
B
Veh
RSM
UMAP2
UMAP1
Subset Name
PMN Ly6C+
PMN F480+
PMN Ly6C+F480+
PMN Ly6C-F480-
CD11b-Ly6G-
CD11b+Ly6C+ Mono
CD11b+F480+ LPM
CD11b+Ly6C-F480-
SigF+ Eos
CD19+ B cell
C
Veh
RSM
%RELMα+
CD11b hi Ly6C-
CD11b int Ly6C-
D
PD-L1 (gMFI)
CD11b+F480+
CD11b-F480-
E
PD-L2 (gMFI)
CD11b+F480+
CD11b-F480-

## Figure 6

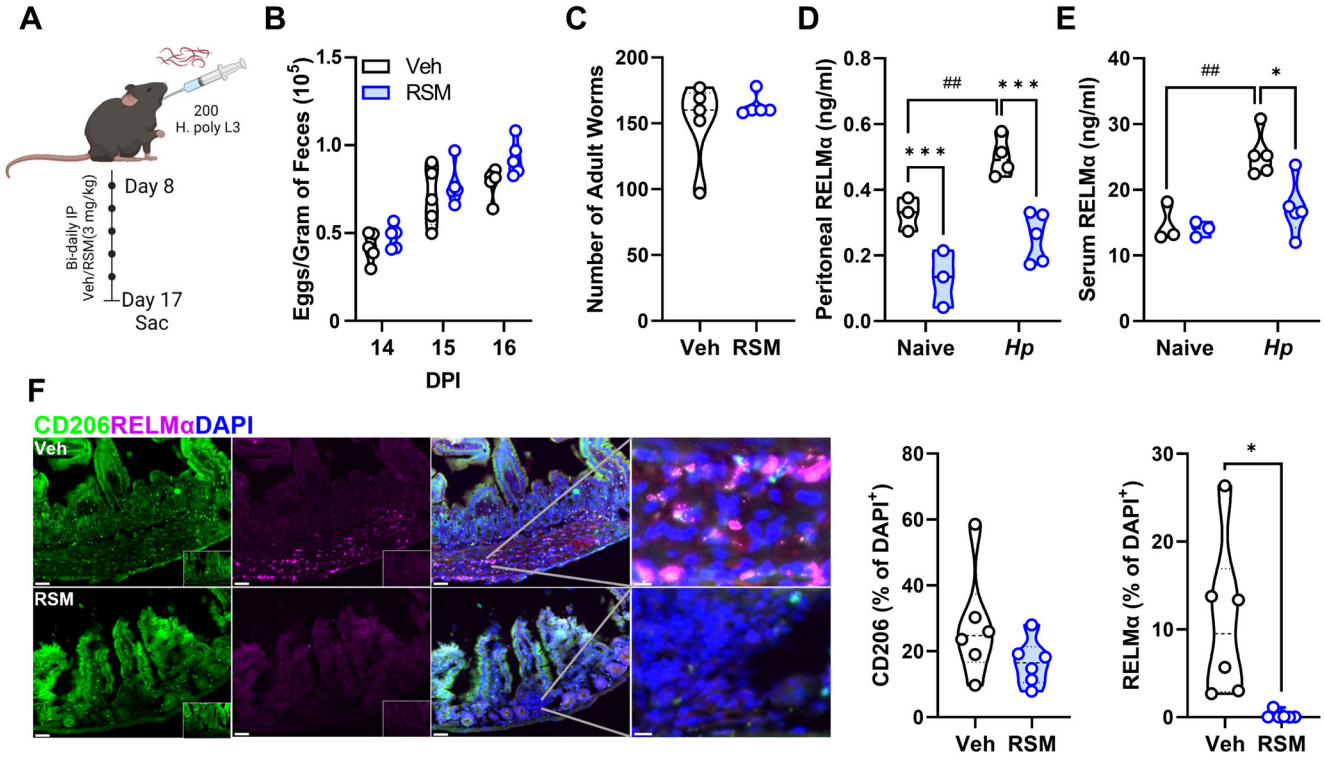
A
200
H. poly L3
Day 8
Bi-daily IP
Veh/RSM(3 mg/kg)
Day 17
Sac
B
Veh
RSM
Eggs/Gram of Feces ($10^5$)
DPI
C
Number of Adult Worms
Veh RSM
D
Peritoneal RELMα (ng/ml)
Naive
Hp
E
Serum RELMα (ng/ml)
Naive
Hp
F
CD206RELMαDAPI
Veh
RSM
CD206 (% of DAPI+)
RELMα (% of DAPI+)
Veh RSM

Figure 7

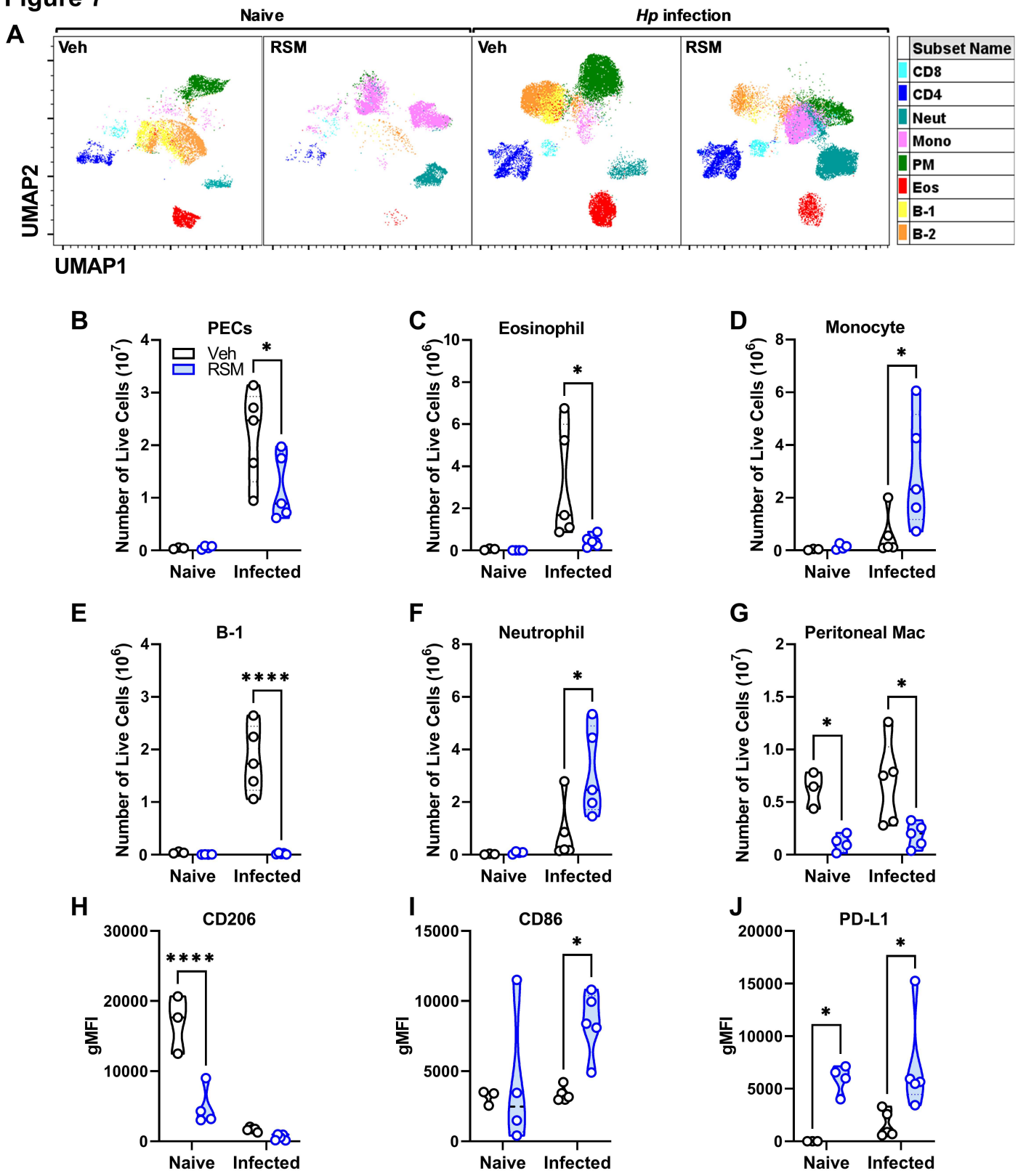
A
Naive
Hp infection
Veh
RSM
Veh
RSM
UMAP2
UMAP1
Subset Name
CD8
CD4
Neut
Mono
PM
Eos
B-1
B-2
B
PECs
Veh
RSM
Number of Live Cells (10^7)
Naive
Infected
C
Eosinophil
Number of Live Cells (10^6)
D
Monocyte
Number of Live Cells (10^6)
E
B-1
Number of Live Cells (10^6)
F
Neutrophil
Number of Live Cells (10^6)
G
Peritoneal Mac
Number of Live Cells (10^7)
H
CD206
gMFI
I
CD86
gMFI
J
PD-L1
gMFI